MRS Communications (2023) 13:1244–1251

https://doi.org/10.1557/s43579-023-00439-x

MRS Communications

Research Letter

Microstructural evolution of 6061 aluminium alloy subjected to static and dynamic compression at low temperature

Mateusz Kopec, Institute of Fundamental Technological Research Polish Academy of Sciences, 5b Pawińskiego Str., 02-106 Warsaw, Poland
Dominika Gorniewicz, Stanisław Jóźwiak, and Jacek Janiszewski, Military University of Technology, 00-908 Warsaw, Poland
Zbigniew L. Kowalewski, Institute of Fundamental Technological Research Polish Academy of Sciences, 5b Pawińskiego Str., 02-106 Warsaw, Poland

Address all correspondence to Mateusz Kopec at **mkopec@ippt.pan.pl**

(Received 30 April 2023; accepted 9 August 2023; published online: 22 August 2023)

Abstract

In this research, an effect of low temperature on the mechanical properties and microstructure of 6061-T6 aluminium alloy (AA6061-T6) subjected to static and dynamic loading was investigated systematically. The specimens were subjected to compression at the temperature of − 80°C in a range of strain rates from 0.001 to 0.1 1/s under static conditions, and from 1250 to 3400 1/s under dynamic conditions to compare their mechanical responses. The deformation mechanisms were discussed based on EBSD analysis. It was found, that under both testing conditions, dynamic recovery was the dominant mechanism responsible for material deformation.

Introduction

Aluminium alloys of the 6xxx series have been widely used in the automotive industry due to their high strength to weight ratio, suitable weldability and machinability, good erosion resistance, and relatively low cost.[1,2] However, the low formability and significant spring back of AA6061 at room temperature limit their ability to form complex-shaped components by using conventional forming technologies.[3] Thus, the low-temperature forming processes were introduced to enhance the formability of aluminium alloys[4] on the one hand, and to avoid severe localized thinning[5] and microstructure deterioration[6] caused by the hot forming on the other.

It was reported, that the forming temperature of − 196°C enable to improve the yield strength, ultimate tensile strength and elongation of AA6060 by approximately 12%, 33% and 48%, respectively.[7] Furthermore, the formability of AA6061 at − 196°C could be enhanced two-fold in comparison to the same conditions at room temperature.[8] A similar deformation behaviour under low temperature was also observed for 7xxx series[9] and 2219[10] aluminium alloys. The microstructural observations revealed, that the dynamic recovery was suppressed at low temperature. This led to an increase of the dislocation density and proportion of screw dislocations. Thus, the enhanced strain hardening rate and simultaneous material strengthening were observed.[11] Moreover, the dislocation was found to be more homogenous at low temperature, resulting in the reduction of slip lines and misorientation.[12] It could be observed, that a susceptibility of aluminium alloys to low-temperature deformation would potentially expand its processing window. However, in order to define it precisely on the industrial scale, a deep understanding of deformation mechanisms is required.

One should highlight, that the feasibility of low-temperature forming of AA5182 aluminium panels[13] and even a dome of rocket with 2 m in diameter[14] were experimentally confirmed. Additionally, the strength and ductility of 5xxx and 6xxx series aluminium alloys increase with a decrease of the temperature from 20 to − 163°C. However, the positive effect of strain rate on the ductility improvement was observed for 5xxx series, only.[15] Schneider et al.[16] highlighted, that the low temperature would be beneficial for aluminium forming. This is due to the lack of strength reduction through the mechanism of recovery, recrystallization and aging induced by forming at higher temperatures after the process. Additionally, the processes of wrinkling and splitting usually taking place during conventional cold and hot forming could be successfully avoided.[14]

Since aluminium alloys have been widely used at low temperature and cryogenic conditions, the knowledge of deformation mechanisms occurring under both, static and dynamic conditions should be expanded. It was also reported, that the application of higher strain rates can potentially improve the efficiency of certain forming processes.[17] As a consequence, deformation mechanisms at high strain rates require systematic thorough investigations. Hence, the microstructural evolution of commercial AA6061 was discussed in this research during low-temperature compression in a wide range of strain rates. The dominant deformation mechanisms were identified using Scanning Electron Microscopy (SEM) and Electron Backscatter Diffraction (EBSD).

Materials and methods

Microstructural characterisation of the as-received AA6061

The microstructure of deformed specimens was characterized using SEM. Prior to the study, the specimens were cold-mounted, and then, polished using Struers MD-Largo disc dedicated to soft materials of 40–150 HV and 9 μm diamond suspension. The polishing process was performed using Metrep® MD-Chem cloth and 0.04 μm Colloidal Silica solution. The microstructural characterization was carried out on the high-resolution Quanta 3D FEG (SEM/FIB) scanning electron microscope system equipped with an integrated EDS/EBSD system (EDS—energy dispersive X-ray detector, and EBSD—electron backscatter diffraction analysis system) operated at 20 kV. The average grain size was calculated using NIS Elements software for the image magnification of ×500.

Experimental details

Static compression tests were performed at strain rates ranging from 0.001 to 0.1 1/s in order to achieve the deformation of approximately 50% at the low temperature of − 80°C using Instron 1343 testing machine equipped with the environmental chamber. High strain rate testing was carried out on the Split Hopkinson Pressure Bar (SHPB) equipped with the low-temperature insulated chamber. It is the most frequently used technique for material testing at high strain rates. SHPB setup consisted of a striker bar, input and output bars, between which a cylindrical specimen was placed. SHPB bars were made of the maraging steel (heat-treated MS350 grade: yield strength – 2300 MPa; elastic wave speed – 4960 m/s). The lengths of the striker, and both, input and output bars, were 250 and 1200 mm, respectively, all with the same diameter of 12 mm. The striker bar was driven by a gas gun with the barrel length of 1200 mm and inner diameter of 12.1 mm. To minimize the wave dispersion and to facilitate stress equilibrium, the copper pulse shapers of 3 mm in diameter and thickness of 0.1, 0.2 or 0.3 mm were used. The dynamic tests at low temperature were conducted in the insulated chamber inside which the cylindrical specimens of 5 mm × 5 mm were cooled down using the liquid nitrogen. The chamber made of high-density polystyrene foam was divided into two parts, upper and lower, to enable its assembly on the Hopkinson bars and the specimen placement between the bars. The chamber was equipped with a window through which the liquid nitrogen was flushed. A thermocouple feedback processing controller was applied to monitor the liquid nitrogen flow using the cryogenic electrovalve. The thermocouple was in contact with the specimen from its upper side, i.e. on the side opposite to the specimen surface, which was cooled by evaporating liquid nitrogen. In this way, the amount of liquid nitrogen flushed into the chamber was controlled to keep a constant temperature for a long time. Based on the preliminary tests on reference specimen (specimen with a small hole in which the thermocouple was placed in the centre of longitudinal specimen axis), it was found out that after reaching a desired level, the temperature was kept constant for at least 5 min to ensure no temperature gradient throughout the specimen. Mechanical properties of the aluminium alloy were characterized for strain rates ranging from 1250 to 3400 1/s and the same temperature of − 80°C. The temperature was selected based on the most extreme, environmental conditions, that could

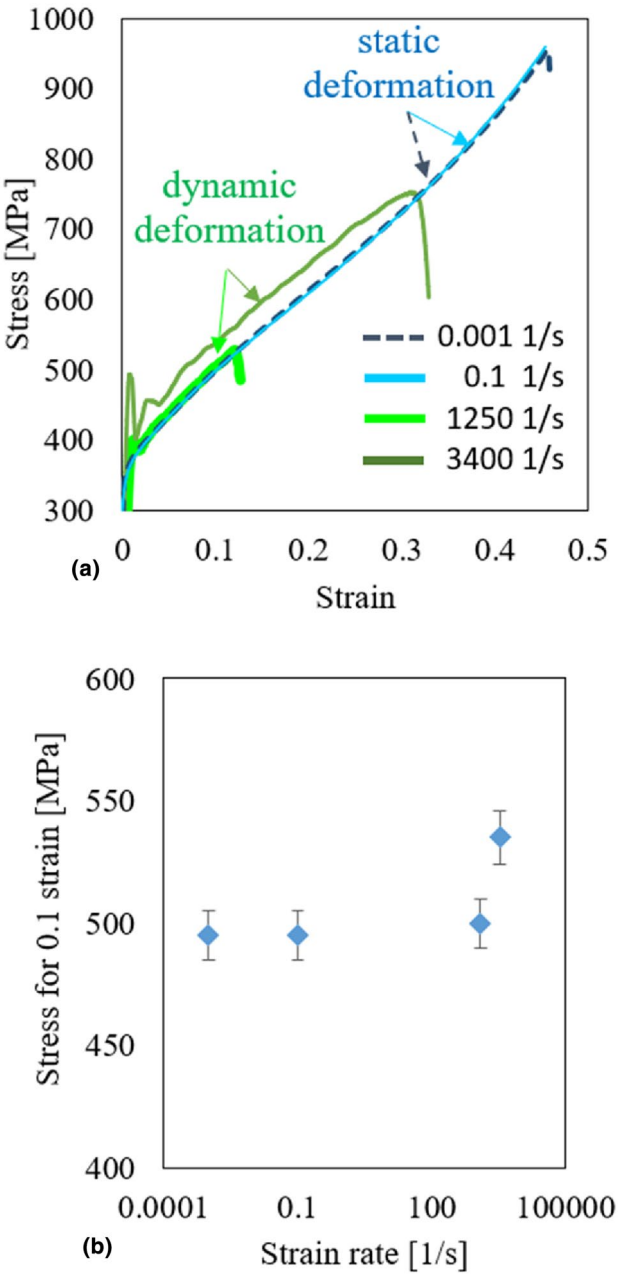

Figure 1. Representative compressive stress–strain characteristics of AA6061 under different values of strain rate and temperature equal to – 80°C (a); stress variations as a function of strain rate (b).

potentially occur in the real applications. Each mechanical test was performed at least twice to check a repeatability of the results. Experiments showed a value of standard deviation less than 5%.

Results and discussion

Low-temperature plastic flow behaviour of AA6061 under compressive loadings in a wide range of strain rates

Figure 1(a) presents the representative stress–strain curves of AA6061 determined from static and dynamic tests at − 80°C. The alloy exhibited a plastic flow stress increase when the strain rate of 3400 1/s was applied. For the rest values of strain rate, the plastic flow stress remained almost constant at strain equal to 0.1, as it is shown in Fig. 1(b). This means, that for the strain rate range from 0.001 to 1250 1/s, the aluminium alloy tested at − 80°C is not strain rate sensitive.

Microstructure evolution of AA6061 subjected to compression at low temperature in a wide range of strain rates

The microstructure of the as-received AA6061 was presented in Fig. 2(a) in the form of an Inverse Pole Figure (IPF), Kernel Average Misorientation (KAM) and Grain Boundaries (GB) maps. The as-received material exhibited equiaxed grains of an average size equal to 50 ± 20 μm without preferred grain orientation. The high fraction of low misorientation may suggest a low dislocation density of material in the as-received state.[18] An evolution of the microstructure was presented in the form of IPF, KAM and GB maps [Fig. 2(b–e)]. One should conclude, that static and dynamic deformation led to a significant increase of low-angle boundaries (LAB) below 5°, since their fraction increased from 0.007 in the as-received state to 0.497 and 0.642 at the strain rate of 0.001 1/s and 1250 1/s, respectively (Table I). It can be also observed, that the static loading leads to the dominant orientation in [111] direction [Fig. 2(b, c)] while for the dynamic one, the [001] orientation seems to be prominent [Fig. 2(d, e)]. Significant differences in KAM maps were also found. The blue colour in these maps represents the low lattice distortion while the orange one the high lattice distortion. The average KAM values tend to increase with increasing level of deformation introduced into the material. It is easy to notice, that higher KAM values are observed at grain boundaries, however, after dynamic deformation at 1250 1/s, some regions of large grains still exhibit areas with relatively low KAM values. Dynamic compression at 3400 1/s as well as static compression performed at strain rates of 0.001 1/s and 0.1 1/s led to the severe deformation of grains with numerous slip bands visible [Fig. 2(b, c)]. However, after dynamic testing, the slip lines were clearly less pronounced and the grains accommodated the process of deformation more evenly, providing a fewer areas of KAM < 3. In order to compare the mechanical response of the aluminium alloy in question, the dynamic tests were repeated at room temperature (RT) under the same strain rate of 1250 1/s and 3400 1/s [Fig. 2(g, i)]. It was observed, that RT deformation leads more likely to slip lines formation, whereas under low-temperature conditions a general reduction of slip lines and a smaller number of highly deformed areas can be observed. An analysis of the relative dislocation density ratio of the material deformed at the same strain rate, but under different values of temperature, enabled to conclude, that the same slip systems were activated during deformation at room and low temperature. Since the material recovery mechanism is more dominant at room temperature, the annihilation process of dislocations should be more effective under the same strain rate applied.[19]

On the contrary, the material hardening is more pronounced at low temperature, therefore, the recovery appears slower.[19] It is related to the fact, that the same number of dislocations is required to reach a certain level of deformation. Thus, for higher temperature (here the room temperature), the material deformation causes the recovery intensification. Furthermore, dislocation generation is constant while dynamic recovery reduces due to temperature lowering. It leads to a higher dislocation density, and therefore, a higher strain hardening rate.[20] Such a phenomenon is responsible for the higher strength of the alloys deformed at low temperature. It was also observed, that shear bands appear more likely in smaller grains (Fig. 2) because the mean free path of dislocations is much shorter in their volume.[17] Since faster blocking of defects occurs at primary grain boundaries, the formation of shear bands can be observed earlier.[21] The shear band formation is a strain rate-dependent phenomenon during which the mechanical energy must be dissipated by the specimen during either static or dynamic deformation.[22] When the highest strain rate of 3400 1/s is considered, a significant amount of energy is introduced to the material. Subsequent generation of heat leads to the intensification of dynamic recovery effects resulting in a decrease of the dislocations number and the shear band formation [Fig. 3(a–d)]. It further causes the more dominant material hardening under dynamic conditions (Fig. 1).[23] The dynamic recovery process in metals, that do not undergo dynamic recrystallization leads to the formation of perfectly ordered, low-energy dislocation systems. The growth of such strongly ordered subboundaries is related to the annihilation and rearrangement of dislocations.[24] An intensive recovery process hinders the accumulation of strain energy, which could potentially accelerate the initiation of dynamic recrystallization.[25] Hardening of the material, before reaching the steady-state plastic flow range, is therefore, associated with an increase of the dislocation density and the formation of a cellular dislocation and sub-grain structures.[26]

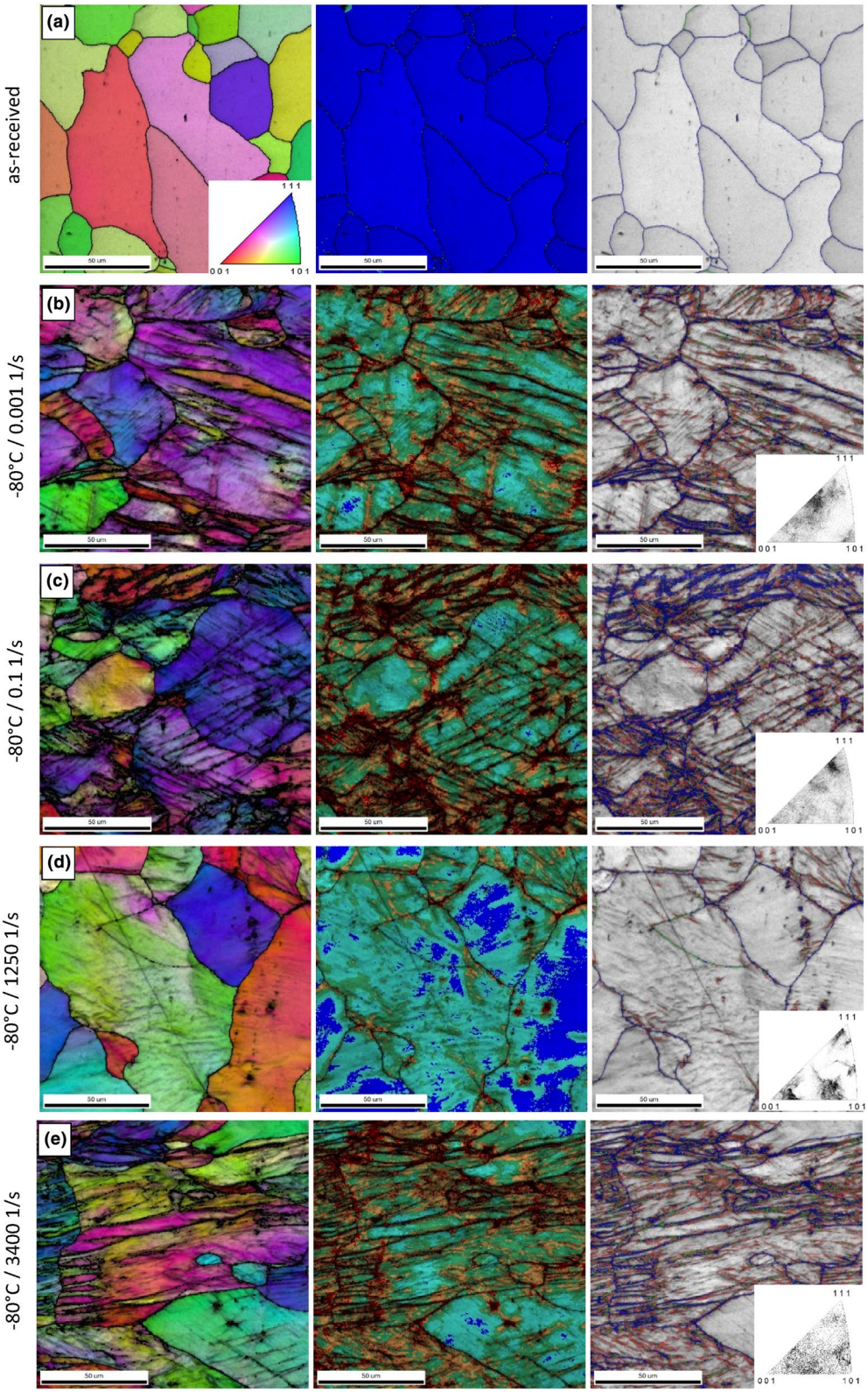

Figure 2. IPF, KAM and GB map of the as-received AA6061 (a); grains after deformation under different values of strain rate: 0.001 1/s (b), 0.1 1/s (c), 1250 1/s (d), 3400 1/s (e); comparison of grain boundaries after deformation at low (f, h) and room (g, i) temperature under different values of strain rate: 1250 1/s (f, g), 3400 1/s (h, i).

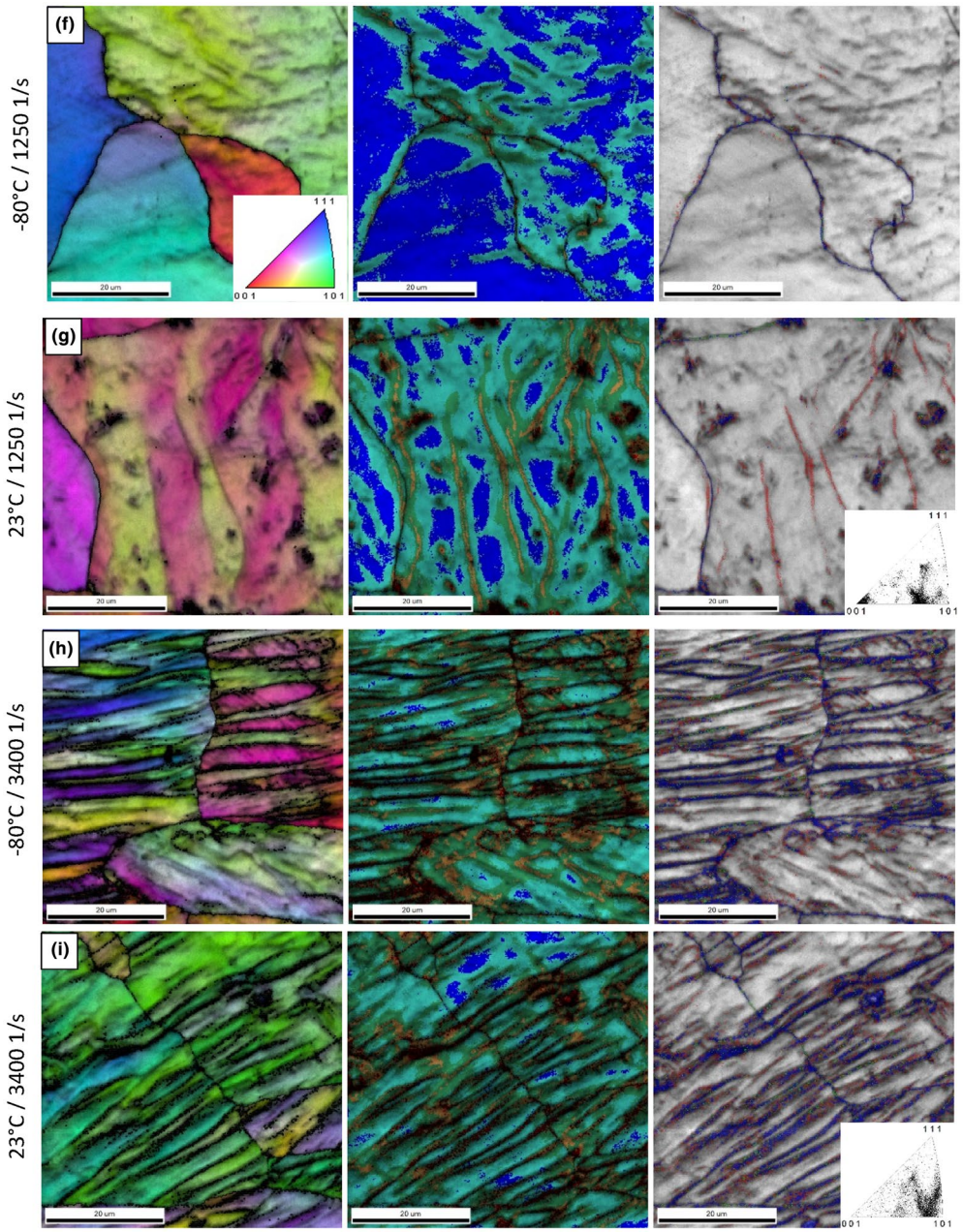

Figure 2. (continued)

Table I. The share of low and high angle boundaries for different strain rates.

	2°–5°	5°–15°	15°–180°
As-received material	0.007	0.032	0.960
0.001 1/s	0.497	0.112	0.391
0.1 1/s	0.413	0.091	0.497
1250 1/s	0.642	0.154	0.204
3400 1/s	0.347	0.155	0.498

Moreover, the dislocation climbing rate during plastic deformation increases with increasing deformation. It is leading to a higher frequency of annihilation, which further enables to reach the equilibrium state.[27] Therefore, the created dislocation substructure and sub-grains are characterized by a similar disorientation angle, which in static conditions would cause further deformation under constant stress. On the other hand, for dynamic processes, the newly formed dislocations are rearranged into new substructures and walls of dislocation cells.[28] One should note, that the average grain size of the as-received AA6061 was 50 μm ± 20 μm and static

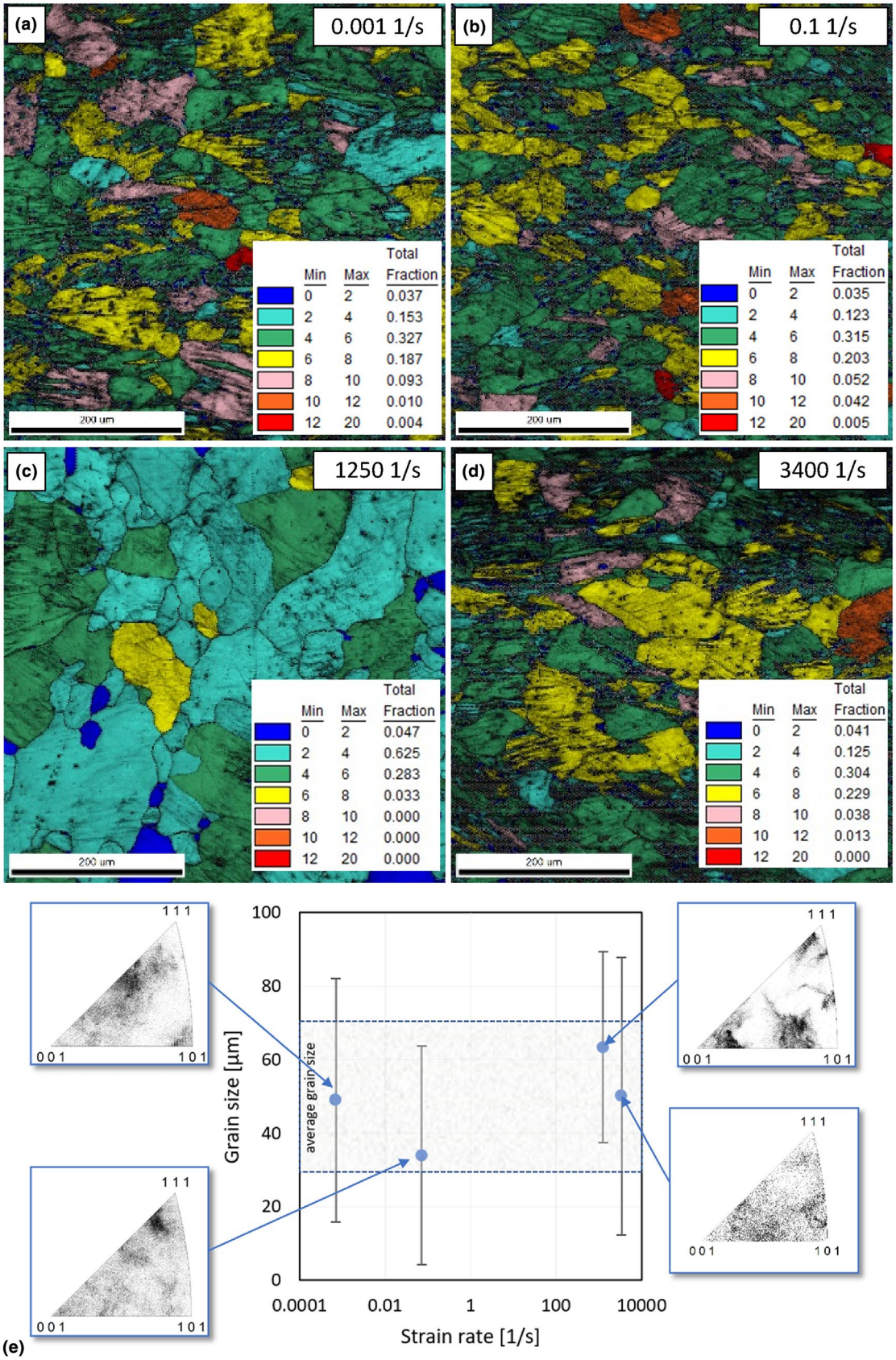

Figure 3. Grain orientation spread after deformation under different values of strain rate: 0.001 1/s (a), 0.1 1/s (b), 1250 1/s (c), 3400 1/s (d); comparison of the average grain size distribution as a function of strain rate at low temperature (e).

and dynamic deformation did not affect its evolution significantly, since only the grain shape was changing, not their equivalent diameter [Fig. 3(e)]. Although a slight grain sizes increase was found under the strain rate of 1250 1/s, their average sizes obtained for the highest strain rate were almost the same as those for the as-received material. Thus, it could be concluded, that in terms of changes of the average grain size, AA6061 is not sensitive to either low or high strain rate deformation under low temperature conditions. However, it should be emphasized, that the orientation of grains changed from [111] under static deformation to [001] after dynamic one.

Conclusions

In this study, the mechanical behaviour of AA6061 was investigated for different values of strain rate at the low temperature equal to − 80°C. Based on the EBSD observations performed, it was found, that the aluminium alloy exhibited relatively low strain rate dependency with the temperature decrease, since the typical stress parameters such as those describing yielding process initiation and maximum stress increased by around 5%. Microstructural analysis indicated that deformation under either low or high strain rate values and low temperature enables to keep constant the material's initial grain size after the loading applied. The main deformation mechanism of aluminium alloy subjected to static and dynamic deformation under low-temperature conditions is represented by dynamic recovery, whose intensity is strain rate-dependent.

Acknowledgments

The author would also like to express his gratitude technical staff—Mr M. Wyszkowski, Mr A. Chojnacki and Mr P. Modrzejewski for their kind help during the experimental part of this work.

Author contributions

MK: conceptualization, MK, DG and JJ: methodology, MK and DG: software, MK, SJ: validation, formal analysis, MK, DG and JJ: investigation, MK and ZK: resources, MK, DG, JJ and SJ: data curation, MK: writing—original draft preparation, ZK: writing—review and editing, MK and DG: visualization, SJ, JJ and ZK: supervision, MK: project administration, funding acquisition. All authors have read and agreed to the published version of the manuscript.

Funding

This research received no external funding.

Data availability

Data available on request.

Declarations

Conflict of interest

The author declares no conflict of interest.

Ethical approval

No animal or human subjects were used in this research.

References

1. M. Zhu, S. Yang, Y. Bai, C. Fan, Mater. Res. Express (2021). https://doi.org/10.1088/2053-1591/abf9cd
2. X. Liu, Z. Cai, Y. Zheng, O. El Fakir, J. Gandra, L. Wang, Appl. Therm. Eng. (2020). https://doi.org/10.1016/j.applthermaleng.2020.115619
3. X. Zhang, Y. Huang, Y. Wang, W. Shen, J. Cui, G. Li, H. Deng, J. Manuf. Process. (2022). https://doi.org/10.1016/j.jmapro.2022.10.058
4. K.E. Lulay, K. Khan, D. Chaaya, J. Mater. Eng. Perform. (2002). https://doi.org/10.1361/105994902770343683
5. H. Gao, O. El Fakir, L. Wang, D.J. Politis, Z. Li, Int. J. Mech. Sci. (2017). https://doi.org/10.1016/j.ijmecsci.2017.07.043
6. A. Talebi-Anaraki, M. Chougan, M. Loh-Mousavi, T. Maeno, J. Manuf. Mater. Process. (2020). https://doi.org/10.3390/jmmp4020056
7. Z. Xu, H.J. Roven, Z. Jia, Mater. Sci. Eng. A (2015). https://doi.org/10.1016/j.msea.2015.09.083
8. X. Wang, X. Fan, X. Chen, S. Yuan, J. Mater. Process. Technol. (2022). https://doi.org/10.1016/j.jmatprotec.2022.117649
9. W. Liu, Y. Hao, Mech. Mater. (2021). https://doi.org/10.1016/j.mechmat.2021.104080
10. X. Fan, X. Chen, S. Yuan, IJMTM (2023). https://doi.org/10.1016/j.ijmachtools.2022.103992
11. D.Y. Park, M. Niewczas, Mater. Sci. Eng. A (2008). https://doi.org/10.1016/j.msea.2008.01.065
12. B. Gruber, F. Grabner, G. Falkinger, A. Schökel, F. Spieckermann, P.J. Uggowitzer, S. Pogatscher, Mater. Des. (2020). https://doi.org/10.1016/j.matdes.2020.108819
13. N. Sotirov, G. Falkinger, F. Grabner, G. Schmid, R. Schneider, R.J. Grant, R. Kelsch, K. Radlmayr, M. Scheerer, C. Reichl, H. Sehrschön, M.

Loipetsberger, Mater. Today: Proc. (2015). https://doi.org/10.1016/j.matpr.2015.05.027
14. F. Xiaobo, Y. Shijian, Int. J. Extrem. Manuf. (2022). https://doi.org/10.1088/2631-7990/ac6b62
15. D.-H. Park, S.-W. Choi, J.-H. Kim, J.-M. Lee, Cryogenics (2015). https://doi.org/10.1016/j.cryogenics.2015.02.001
16. R. Schneider, B. Heine, R.J. Grant, Z. Zouaoui, IOP Conf. Ser. Mater. Sci. Eng. (2015). https://doi.org/10.1088/1757-899X/74/1/012014
17. K. Wang, M. Kopec, S. Chang, B. Qu, J. Liu, D.J. Politis, L. Wang, G. Liu, Mater. Des. (2020). https://doi.org/10.1016/j.matdes.2020.108948
18. S.-S. Rui, Q.-N. Han, X. Wang, S. Li, X. Ma, Y. Su, Z. Cai, D. Du, H.-J. Shi, Mater. Today Commun. (2021). https://doi.org/10.1016/j.mtcomm.2021.102445
19. B. Gruber, F. Grabner, W. Fragner, A. Schökel, F. Spieckermann, P.J. Uggowitzer, S. Pogatscher, Materials (2020). https://doi.org/10.3390/ma13030554
20. B. Gruber, I. Weißensteiner, T. Kremmer, F. Grabner, G. Falkinger, A. Schökel, F. Spieckermann, R. Schäublin, P.J. Uggowitzer, S. Pogatscher, Mater. Sci. Eng. A (2020). https://doi.org/10.1016/j.msea.2020.139935
21. R. Gautier, A. Rajabzadeh, M. Larranaga, N. Combe, F. Mompiou, M. Legros, C R Phys. (2021). https://doi.org/10.5802/crphys.52
22. W. Nowacki, Z. Nowak, P. Perzyna, R. Pęcherski, J. Theor. Appl. Mech. **48**(4), 1003–1026 (2010)
23. L. Su, G. Deng, V. Luzin, H. Wang, Z. Wang, H. Yu, H. Li, A.K. Tieu, Mater. Sci. Eng. A (2020). https://doi.org/10.1016/j.msea.2020.139190
24. T. Sakai, A. Belyakov, R. Kaibyshev, H. Miura, J.J. Jonas, Prog. Mater. Sci. (2014). https://doi.org/10.1016/j.pmatsci.2013.09.002
25. K.K. Alaneme, E.A. Okotete, J. Sci.-Adv. Mater. Dev. (2019). https://doi.org/10.1016/j.jsamd.2018.12.007
26. J. Wanni, J.G. Michopoulos, A. Achuthan, Addit. Manuf. (2022). https://doi.org/10.1016/j.addma.2022.102603
27. A.A. Kohnert, L. Capolungo, NPJ Comput. Mater. (2022). https://doi.org/10.1038/s41524-022-00790-y
28. H.E. Sabzi, E. Hernandez-Nava, X.-H. Li, H. Fu, D. San-Martín, P.E.J. Rivera-Díaz-del-Castillo, Mater. Des. (2021). https://doi.org/10.1016/j.matdes.2021.110246